Available online at www.sciencedirect.com
ScienceDirect
Acta Materialia 56 (2008) 2363–2373
Acta MATERIALIA
www.elsevier.com/locate/actamat

Five-parameter grain boundary distribution of commercially grain boundary engineered nickel and copper

V. Randle [a,*], G.S. Rohrer [b], H.M. Miller [b], M. Coleman [a], G.T. Owen [a]

[a] *Materials Research Centre, School of Engineering, University of Wales Swansea, Swansea, UK*
[b] *Department of Materials Science and Engineering, Carnegie Mellon University, Pittsburgh, PA 15213-3890, USA*

Received 26 February 2007; received in revised form 14 January 2008; accepted 16 January 2008
Available online 5 March 2008

Abstract

The five-parameter grain boundary distributions of grain boundary engineered nickel and copper specimens have been analyzed in detail. The relative areas of {1 1 1} planes in the entire population did not increase as a result of grain boundary engineering (GBE) and, in the Σ3-excluded population, decreased after GBE. This decrease occurred because the majority of the newly generated Σ3 grain boundaries were not coherent twins with {1 1 1} grain boundary plane orientations. GBE increased the proportion of Σ3 boundary length that was vicinal-to-{1 1 1} and the proportion of asymmetrical ⟨1 1 0⟩ tilt boundaries. There was a clear propensity for selection of particular planes or plane combinations which were associated with low energy. These plane types were analyzed in some detail, and it was shown that many of these boundaries were asymmetrical tilts comprising (or vicinal to) at least one low-index plane.

Keywords: Grain boundary; Grain boundary twin; Electron backscatter diffraction; Grain boundary plane

1. Introduction

Grain boundary engineering (GBE) is the deliberate manipulation of grain boundary structure in order to improve material properties such as corrosion resistance, intergranular cracking or ductility. GBE exploits prolific annealing twinning in low stacking-fault energy metals and alloys. Recently GBE in this class of materials has been reviewed [1] and discussed [2] in detail. With reference to the coincidence site lattice (CSL) nomenclature, twins are one type of Σ3 boundary. A commercial grain boundary engineered material is required to have more than 50% Σ3 boundaries (as a fraction of the total number of boundaries) in the interface population [3].

The profuse annealing twinning associated with GBE gives rise to "multiple twinning", whereby two Σ3 boundaries meet at a triple junction and produce a Σ9 boundary, which can be expressed as $\Sigma3 + \Sigma3 \rightarrow \Sigma9$. Higher order $\Sigma3^n$ boundaries are similarly generated, e.g., $\Sigma3 + \Sigma9 \rightarrow \Sigma27$. Because so many Σ3s exist in the microstructure, these reactions also happen in reverse, e.g., $\Sigma3 + \Sigma9 \rightarrow \Sigma3$. The generalized expression of this concept is the "Σ3 regeneration mechanism", which states that $\Sigma3^n + \Sigma3^{n+1} \rightarrow \Sigma3$, is observed more frequently at triple junctions than $\Sigma3^n + \Sigma3^{n+1} \rightarrow \Sigma3^{n+2}$ [4]. The $\Sigma3 + \Sigma9$ reaction can of course also result in a Σ27 [5]. Increasingly, cluster statistics derived from percolation theory are also being used to add value to descriptions of GBE processing (e.g., [6]).

The central feature of the regeneration mechanism model is that the new Σ3s are essentially not annealing twins and are therefore not on {1 1 1} interface planes. Rather, they could occupy a variety of boundary planes. Σ3 boundary planes other than {1 1 1} are highly mobile and would therefore promote further encounters with other Σ3s, hence perpetuating Σ3 regeneration. The mobile Σ3s in the grain boundary engineered specimen would become directly incorporated in the grain boundary network and break up the remaining random boundaries, hence leading to the improved intergranular properties associated with

* Corresponding author. Tel./fax: +44 1792 29 5.
E-mail address: v.randle@swansea.ac.uk (V. Randle).

1359-6454/$34.00
doi:10.1016/j.actamat.2008.01.039

grain boundary engineered metals. To date, the Σ3 regeneration model has not been fully validated by measurement of interface planes in an appropriately grain boundary engineered specimen. Although there are many reports of misorientation statistics associated with grain boundary and GBE investigations, measurements of boundary planes are far more sparse. Some previous investigations on the distribution of Σ3 boundary planes in copper and nickel have shown that the population comprises a high proportion of planes vicinal to {1 1 1} on the ⟨0 1 1⟩ zone (such as {23, 17, 17}/{7 7 5}) and other asymmetric tilt boundaries on the ⟨1 1 0⟩ zone, as well as coherent twins on {1 1 1} [7]. These results accord well with data to show the energy of Σ3 misorientations as a function of deviation from {1 1 1} [8].

Recently, a new stereological technique for measuring the five-parameter grain boundary distribution (FPGBD), which is described in detail elsewhere [9], has been developed to provide statistical data on the distribution of boundary planes in addition to misorientations. Results from analyses using the five-parameter technique, for example on magnesium oxide and on aluminium, have contributed to a growing body of evidence which suggests that special behaviour at grain boundaries is related to low-index planes rather than particular misorientations (e.g., [10,11]). A selection of other studies on the relationship between the boundary plane and boundary properties is summarized elsewhere [12].

In the present study, we measure the FPGBD of commercially grain boundary engineered copper and nickel [13]. We also assess the intergranular corrosion of both grain boundary engineered and control specimens. Elsewhere there is an increasing number of cases in the recent open literature of property benefits brought about by GBE processing. For example, a direct correlation has been shown between intergranular stress corrosion cracking and proportion of CSL boundaries in austenitic alloys [14], and GBE processing has been used to improve the thermal stability of Inconel alloy 617 [15]. The data here will be interpreted with particular emphasis on the distribution of boundary planes present and its consequences for our understanding of GBE.

2. Experimental methods

All the specimens were obtained from Integran Technologies, Inc. The nickel samples were provided in a reference state (before GBE) and in a final state following the GBE process. The two samples will be referred to as non-GBE nickel and GBE nickel, respectively. The samples were prepared by first grinding the surface with SiC and diamond abrasives, then polishing using a vibratory chemomechanical process with a 0.05 μm SiO_2 slurry, and finally electropolishing in a chilled 9:1 methanol:perchloric acid solution.

Crystal orientation maps on planar sections were obtained using an electron backscatter diffraction (EBSD) mapping system integrated with a scanning electron microscope. The step sizes for the orientation mapping were between 2 and 4 μm, and were recorded over individual areas of 1–4 mm^2. In total, 64.0 mm^2 of the non-GBE sample were mapped (an area containing approximately 20,000 grains) and 67.3 mm^2 of the GBE sample were mapped (an area containing approximately 25,000 grains). The orientation data were then processed to remove spurious observations using a "grain dilation clean-up" function in the orientation imaging microscopy (OIM) software. A single orientation was then assigned to each grain by averaging all of the orientations belonging to a single grain. The OIM analysis software was then used to extract 86,335 boundary line traces from the reference sample and 115,231 traces from the GBE sample. The FPGBD was determined from these traces using a procedure described previously [16]. Part of the procedure is segmentation of curved grain boundaries. The Brandon criterion was used to classify $\Sigma 3^n$ boundaries, with $n \leqslant 3$, i.e., Σ3, Σ9 and Σ27, as a fraction of total boundary length. The proportion of misorientations on specific axes ([0 0 1], [1 1 0], [1 1 1]) was calculated with a tolerance of ±5°. The accuracy of a misorientation measurement obtained by EBSD is 0.5°. The FPGBD is presented as a multiples of a random distribution (MRD) which corresponds to relative areas. The resolution of the distribution is approximately 10° and all distributions are plotted in stereographic projection.

The GBE copper specimens, also obtained from Integran Technologies, Inc., were prepared in a similar manner to the nickel specimens, except that the etchant was 50:50 ammonia and hydrogen peroxide immersion for 3–5 s. A 0.5 μm step size was used, and 62,147 grain boundary line traces were extracted from the data. The data were then processed as described above. The copper specimens, both before and after GBE, were immersed for both 1.5 and 48 h in a modified Livingston's reagent.

3. Results

The proportions of Σ3, Σ9 and Σ27 boundaries in the non-GBE and the GBE nickel are shown in Fig. 1. For ease of reference throughout this section, we will describe first

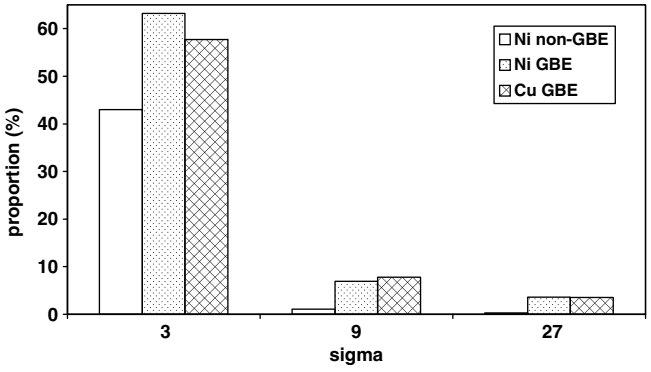

Fig. 1. Length fractions of Σ3, Σ9 and Σ27 boundaries in the non-GBE nickel, GBE nickel and GBE copper specimens.

the data from nickel (non-GBE and GBE), and afterwards compare it with that from copper. There is a large increase in the Σ3 and Σ9 proportion as a consequence of GBE processing: 63% of interface length is Σ3, compared to 43% before GBE. A substantial increase in Σ9s from 1% to 6.9% by length has accompanied the Σ3 increase, and Σ27s have likewise increased as a consequence of GBE. Grain boundaries with CSL misorientations other than Σ3, Σ9 and Σ27 (i.e., $\Sigma 3^n$) are not present at levels above those expected for a random distribution.

The microstructure of both the non-GBE and the GBE nickel is shown in Fig. 2. Before GBE, grains were equiaxed and annealing twins were long and straight – a typical microstructure of an annealed medium stacking fault energy metal. After GBE, Σ3s have a convoluted morphology and the extensive Σ3 population has broken up the random boundary network. This microstructure is typical of a GBE metal where Σ3 regeneration has taken place. Note that whereas the total grain boundary length per unit area is approximately the same in the two samples (3.4×10^{-2} and $3.5 \times 10^{-2}\,\mu m^{-1}$ in the non-GBE and GBE sample, respectively), GBE results in a significant decrease in the length of random grain boundaries per unit area that is compensated for by the creation of new $\Sigma 3^n$ grain boundaries. The microstructure of the copper specimens was very similar to that of the nickel specimens except that the grain size was smaller in the former.

The relative area distributions of interface planes are plotted in standard stereographic projection in Figs. 3–6. In all of the projections, the [0 0 1] crystal axis is perpendicular to the plane of the paper and the [1 0 0] direction is horizontal in the plane of the paper and pointing to the right. Fig. 3a and b show the overall distribution of boundary planes for the entire sample population. Maxima are centred on {1 1 1} and minima, where the density is less than that expected in a random distribution, are centred on {1 0 0}. The relative areas of planes with {1 1 1} is approximately the same before and after GBE (namely 5.30 MRD compared to 5.17 MRD). In Fig. 3d and e, Σ3 misorientations have been excluded from the statistics on the grounds that two-thirds of the interface length is Σ3, which dominates the distribution. When Σ3 boundaries are excluded, the form of the distribution remains the same but the {1 1 1} maxima drop to 1.44 and 1.29 MRD for non-GBE and GBE nickel, respectively. The drastic reduction in the population from more than 5 MRD to less than 1.5 MRD reflects the fact that most of the Σ3 boundaries subtracted from the population are coherent twins on {1 1 1} planes.

Grain boundary plane distributions for misorientations about the [1 1 0] axis are shown in Fig. 4. The grain boundary plane distributions at misorientations about [1 1 1] are shown in Fig. 5 and the distributions for the Σ27b boundaries are shown in Fig. 6. In the calculation of these distributions, the Σ3 boundaries were excluded, so they can be thought of as the relative populations of all non-Σ3 boundaries. Grain boundary plane distributions for [1 0 0] misorientations have also been examined, but are not presented here because less than 1% of the boundary length is misoriented on this axis and furthermore the distributions do not greatly deviate from random.

It can be seen that GBE processing has modified the distribution of grain boundary planes for boundaries with [1 1 0] and [1 1 1] misorientations. The general characteristics can be summarized in the following way. For [1 1 0] misorientations, grain boundary plane orientations in the [1 1 0] zone (pure tilt boundaries) are preferred, for grain boundaries with [1 1 1] misorientations grain boundary planes with [1 1 1] orientations are preferred (pure twist boundaries) and for low misorientation angle boundaries (10° about [1 1 0] or [1 1 1]) mixed boundaries are most frequently adopted.

The predominant maxima along the [1 1 0] zone (Fig. 4) indicate that most of the segments have tilt character. In all

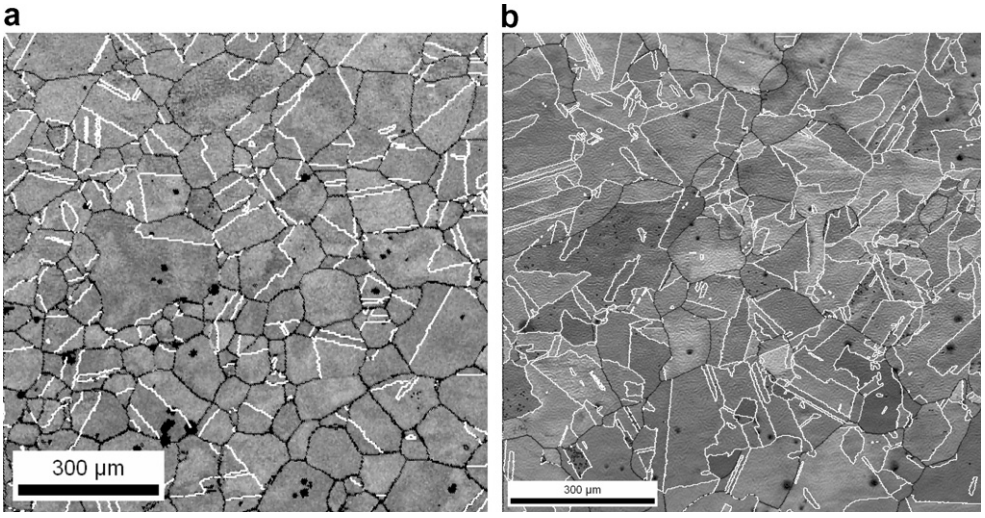

Fig. 2. Microstructures of (a) non-GBE and (b) GBE Ni. Σ3 boundaries are grey and all other interfaces are black. The background represents a measure of diffraction pattern quality where the black spots are blemishes on the specimen surface.

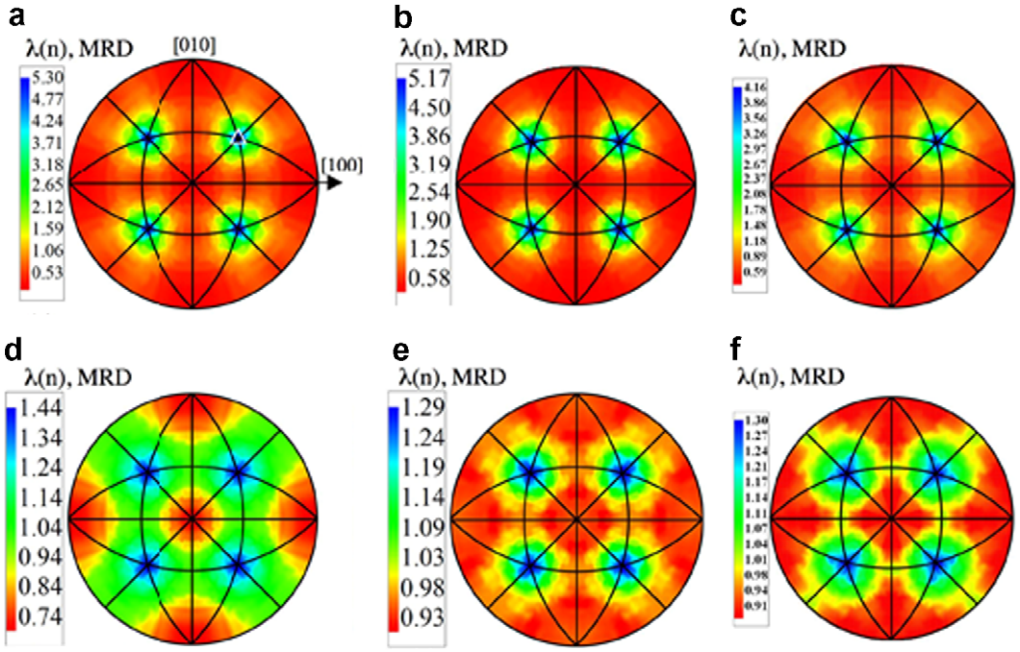

Fig. 3. The relative areas of boundary planes for the entire grain boundary population, in MRD units, for the non-GBE nickel (a), GBE nickel (b) and GBE copper specimens (c). The relative areas of boundary planes, excluding Σ3 grain boundaries, for non-GBE nickel (d), GBE nickel (e) and GBE copper specimens (f). The [1 1 1] direction is denoted by white triangle and the [1 0 0] direction by a black arrow (a). This reference frame is used on all subsequent figures.

cases, maxima are several times greater than the random distribution value of unity. There are some significant differences between the non-GBE and the GBE nickel. Whereas in both cases the maximum MRD values occur for the Σ9 and Σ27a misorientations, the MRD values are much higher for the GBE nickel (up to 27 MRD) than for the non-GBE nickel (up to 6.5 MRD). These results correspond to the high level of multiple twinning after GBE. In general, the misorientations on [1 1 0] have a strong tendency to exist as asymmetrical tilt boundaries (ATGB), i.e., there are multiple peaks on the [1 1 0] zone. These peaks are frequently overlapping, as illustrated in Fig. 7.

The distributions of interface planes for boundaries with [1 1 1] misorientation axes, Fig. 5, show a preference for (1 1 1) twist boundaries. The propensity for twist character is much stronger in the non-GBE nickel than in the GBE nickel. However, the significance of these results is tempered by the fact that less than 2% of grain boundary length (excluding Σ3) is misoriented on [1 1 1].

The distributions of grain boundary planes for the exact Σ9, Σ27a and Σ27b misorientations (38.94°/⟨1 1 0⟩, 31.58°/⟨1 1 0⟩ and 35.42°/⟨2 1 0⟩, respectively) are shown in Figs. 4 and 6. We will now describe these three misorientations in turn. In the section for Σ9 there are two maxima, near (1 −1 1) and (−1 1 5), which represent planes on the [1 1 0] zone. To show this clearly, the data along the tilt section have been extracted and are plotted in Fig. 7a. The maxima are diffuse and include the {1 1 1}/{1 1 5} asymmetric tilt boundary and other ATBGs in the Σ9 system. There is also a local maximum on the tilt zone corresponding to the symmetrical tilt boundary (1 −1 4). Note that the minimum along the tilt zone is found at the symmetric (−2 2 1) orientation. For the non-GBE nickel the maxima on the 1 1 0 zone are more diffuse, with a local minimum at the symmetric (1 −1 4) and an absolute minimum at the symmetric (−2 2 1) orientation.

For Σ27a boundaries there are three rather broad maxima in the GBE specimen. These look very similar to the Σ9 case except that, because of the smaller misorientation angle, the peaks are displaced along the [1 1 0] zone in the Σ27a case. The planes closest to the maxima are the asymmetric pair (−1 1 7)/(2 −2 3). Σ27b boundaries are seen to be aligned close to the [1 1 0] zone, even though the misorientation axis is [2 1 0] and not [1 1 0]. An explanation for this is that the disorientation is symmetrically equivalent to the boundary obtained by a 146° rotation about the [7 7 1] axis and, because this direction is only 5.8° from [1 1 0], the zone of tilts is very near [1 1 0]. The preference for grain boundary planes in the [1 1 0] zone for the Σ27b boundary suggests that grain boundary planes in this zone have relatively low energy, even when they are not pure tilt boundaries. In the non-GBE nickel the distribution for Σ27b is closer to random.

Turning now to the GBE copper, the distribution is broadly similar to that of GBE nickel, with some subtle yet significant differences. These are summarized as follows. There are 58% Σ3 in the GBE copper compared to 63% in the GBE nickel, and the Σ9 and Σ27 proportions are nearly the same (Fig. 1). The microstructures of the two specimens have a similar morphology, but grain size in the copper specimen is smaller than that of the nickel

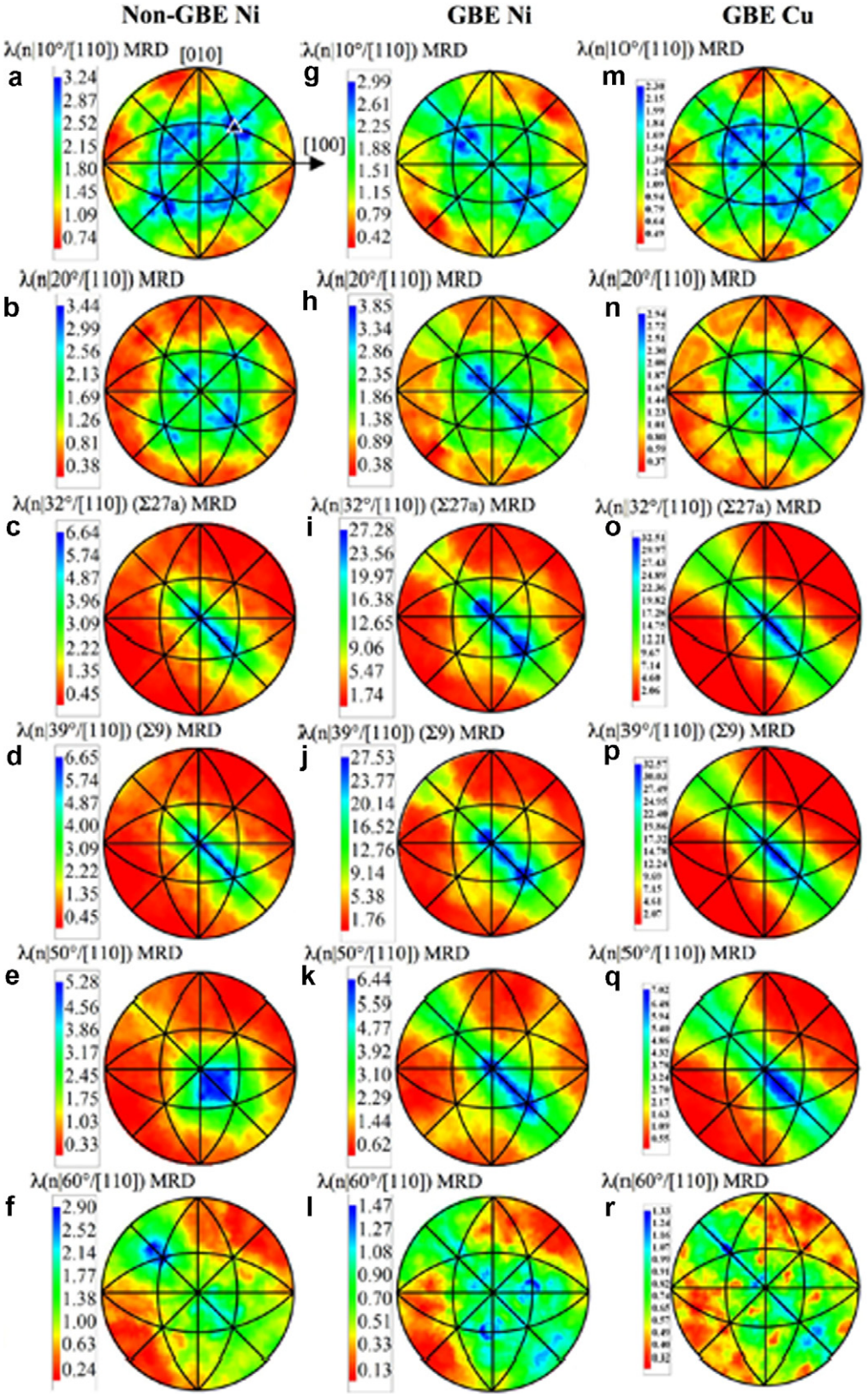

Fig. 4. The relative areas boundary planes for grain boundaries misoriented on [1 1 0], expressed as "multiples of a random distribution" (MRD) for the non-GBE nickel (a–f), GBE nickel (g–l) and GBE copper (m–r) specimens. For each case, rotation angles are indicated in the legend.

specimen. There are fewer {1 1 1} planes in the overall distribution of copper compared to nickel (4.16 MRD compared to 5.17 MRD) (Fig. 3c). However, when Σ3 boundaries are excluded the distribution is very similar,

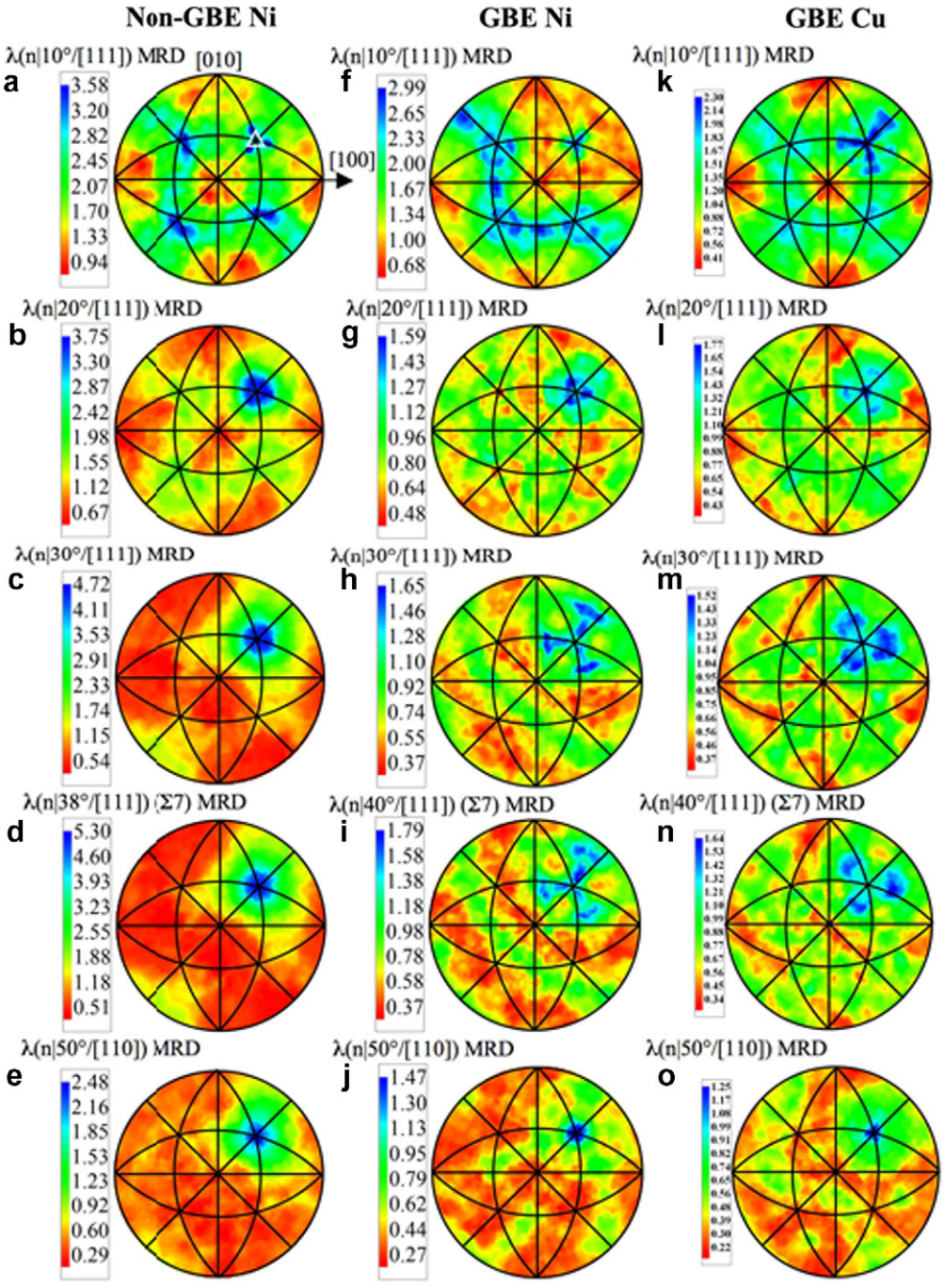

Fig. 5. The relative areas boundary planes for grain boundaries misoriented on [1 1 1], expressed as ''multiples of a random distribution'' (MRD) for the non-GBE nickel (a–e), GBE nickel (f–j) and GBE copper (k–o) specimens. For each case, rotation angles are indicated in the legend.

i.e., in the non-Σ3 grain boundary population the relative area of {1 1 1} planes is greater than expected in a random distribution (Fig. 3f).

The distribution of boundaries misoriented on [1 1 0] is similar in both GBE specimens, namely it is composed of tilt boundaries with similar peak MRD values (Fig. 4m–r). The distribution of boundaries misoriented on [1 1 1] is similar in terms of MRD value, whereas slightly different planes are represented in the two specimens (Fig. 5). In the GBE copper the Σ9 misorientation (maximum MRD 32.6) is similar to that for nickel, but the maxima appear to be confined more narrowly on the [110] zone. The Σ27a and Σ27b distributions are broadly similar for both GBE copper and nickel, although there are different planes represented on or near the [1 1 0] zone in the two cases.

The distributions of triple junction types have also been calculated, based on the misorientations of the boundaries which comprise the junction. For this purpose boundaries are classified as Σ3, Σ9, Σ27 or random (R). The proportions of boundary combinations (where the proportion exceeds 1% of total junctions) at junctions are shown in Fig. 8. Whereas the distributions for GBE nickel and

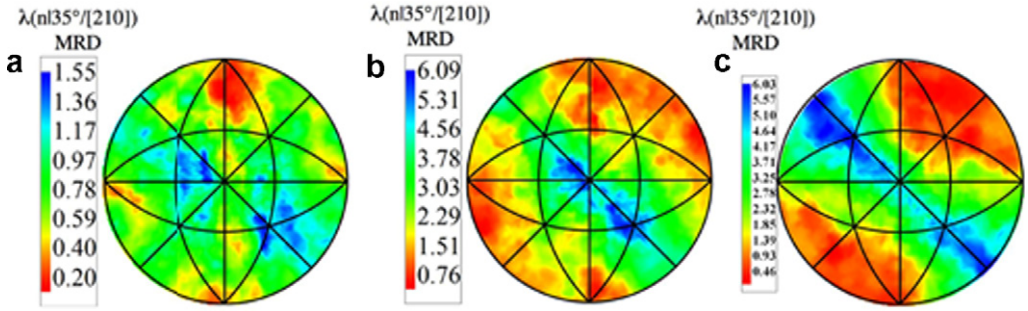

Fig. 6. The relative areas of boundary planes Σ27b grain boundaries, expressed as "multiples of a random distribution" (MRD) for the non-GBE nickel (a), GBE nickel (b) and GBE copper (c) specimens.

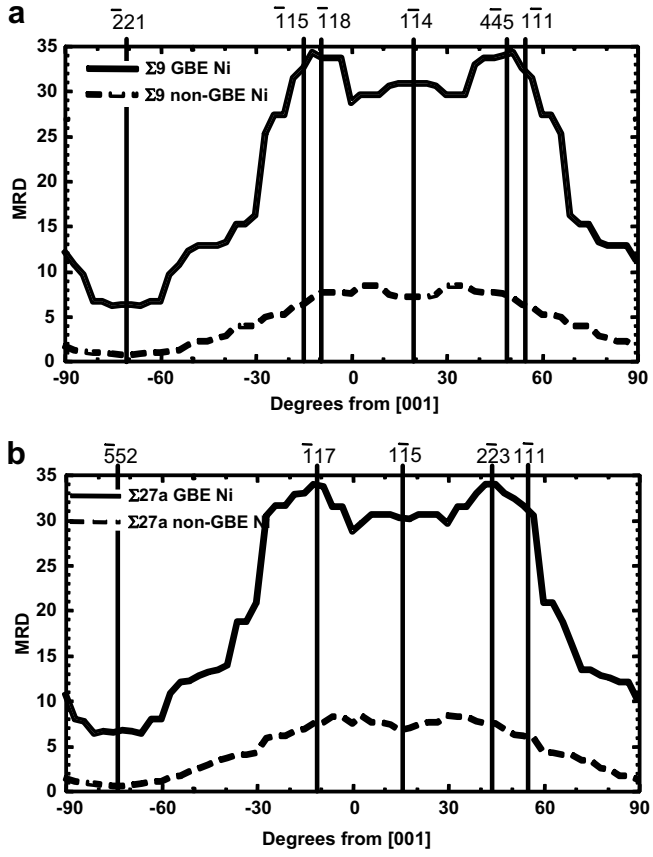

Fig. 7. Grain boundary plane populations for orientation along the [1 1 0] zone for the Σ9 (a) and Σ27a (b) misorientations.

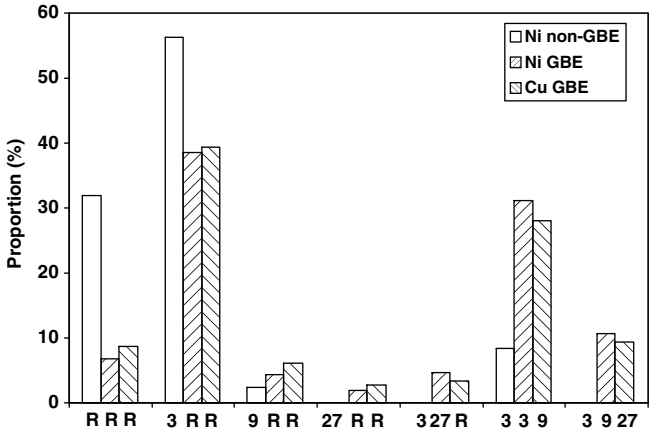

Fig. 8. Proportions of triple junction types for the non-GBE nickel, GBE nickel and GBE copper specimens. Triple junctions are defined according to Σ3, Σ9 Σ27 or random (R) boundaries.

copper specimens are very similar, there is a dramatic difference between the non-GBE and the GBE nickel. Before GBE, most of the junctions are either Σ3–R–R (56%) or R–R–R combinations (32%). After GBE the Σ3–R–R category has reduced to 39% whereas 42% of junctions are now either Σ3–Σ3–Σ9 or Σ3–9–Σ27.

Finally, the success of the GBE was verified here by exposure of both the GBE and reference specimens to a corrosive medium, namely modified Livingston's reagent. The corrosive attack on the specimens after 1.5 h exposure is recorded in Fig. 9. Here it can be clearly seen that the intergranular attack on the copper reference specimen is widespread (Fig. 9a), whereas the intergranular attack on the GBE copper specimen, for the same duration, is considerably less (Fig. 9b). Moreover the two specimens were immersed in the reagent for a longer period, namely 48 h, in order to record the specimen weight loss as a consequence of corrosive attack. The reference specimen lost 19.2% of its original weight and the GBE specimen lost less weight, 15.8%. These results validate the success of the GBE processing in terms of resistance to intergranular corrosion.

Fig. 9c shows an enlarged portion of a corroded area on the GBE copper specimen accompanied by an orientation map of the same area (Fig. 9d). Here Σ3, Σ9 and Σ27 boundaries are red, blue and yellow, respectively, and random boundaries are black. Almost all of the Σ3 boundary length is unattacked by the etchant, whereas other boundaries, including Σ9 and Σ27, are corroded. Small segments of Σ3 boundary that have been corroded are arrowed. The faceted nature of the corroded parts indicates a relationship with the boundary plane indices. However, most Σ3 facets remain uncorroded, which shows that the GBE is a direct result of a large fraction Σ3 boundary which substitutes for random boundaries in the grain boundary network.

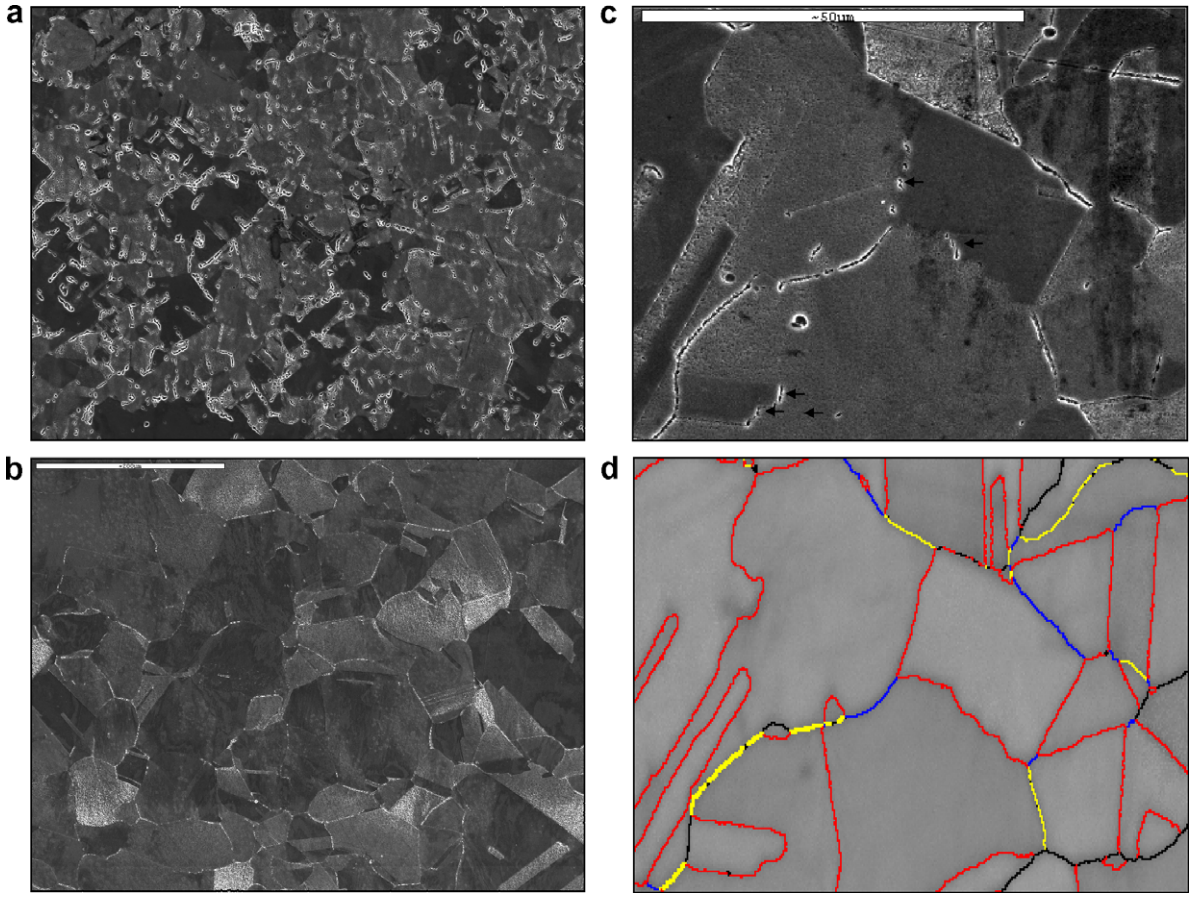

Fig. 9. GBE copper specimens having been exposed to Livingston's modified reagent for 1.5 h. (a) Reference copper specimen; (b and c) GBE copper specimen; (d) orientation map of the region in (c). Σ3, Σ9, Σ27 and random boundaries are red, blue, yellow and black, respectively. In (c) small segments of Σ3 which have corroded are arrowed. (For interpretation of the references in colour in this figure legend, the reader is referred to the web version of this article.)

4. Discussion

In both copper and nickel the most common plane present is the plane with lowest surface energy, {1 1 1} (Fig. 3). This tendency for boundaries to terminate on low surface energy planes, which assumes that frequency of occurrence is inversely related to energy, has been previously observed in materials having a variety of crystal structures [10,11]. Such surfaces have low indices. For face-centred cubic (fcc) materials, the dominance of {1 1 1} boundary planes has been previously recorded in aluminium [11] and brass [14], and so the present data further confirm this preponderance of low surface energy planes as a general trend. However, a surprising result in the present data is that, even though the proportion of Σ3 misorientations in the nickel specimens increased by approximately 50% as a consequence of GBE, the relative areas of {1 1 1} planes after GBE did not increase and, in the Σ3-excluded population, actually decreased after GBE processing.

The decrease in {1 1 1} planes after GBE indicates that most of the additional Σ3 population were not newly generated, coherent annealing twins, because these would have been on {1 1 1}. The convoluted morphology of the Σ3 boundaries as seen in Fig. 2b suggests that many of the planes are not on {1 1 1}. However, even though this type of morphology is commonly observed in a Σ3-regenerated GBE microstructure, the identity of the planes has never actually been revealed before. The contour distribution of planes for the 70.53°/[1 1 0] misorientation (a Σ3 symmetrically equivalent misorientation to 60°/[1 1 1]) is shown in Fig. 10 for both the non-GBE and the GBE nickel. The MRD maxima for these misorientations before and after GBE were 1212 and 1428, respectively. It is apparent that there is a broader spread about {1 1 1} in the distribution after GBE. These planes are therefore not all {1 1 1}, and are instead either vicinal-to-{1 1 1} or other ATGBs, which could both be formed by Σ3 regeneration. Multiple twinning and Σ3 regeneration has also led to a substantial increase in Σ9s after GBE. The data here are in contrast to a recent five-parameter analysis on iteratively processed brass, where the proportion of {1 1 1} planes increased after the processing. In the brass case the proportion of Σ3 increased to a similar level to that observed here; however, the increase was mostly in the form of new annealing twins, which accounted for the increase in {1 1 1} population [15].

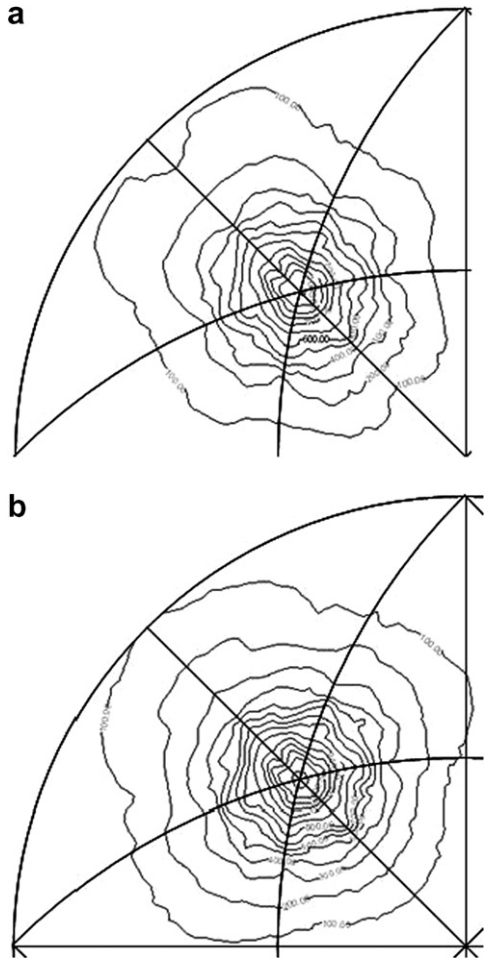

Fig. 10. Contour distributions of planes for the 70.53°/[1 1 0] misorientation (a Σ3 symmetrically equivalent misorientation to 60°/[1 1 1]) for (a) non-GBE and (b) GBE nickel. The contours are in steps of 100 MRD.

If one considers only the Σ3, Σ9 and Σ27a boundaries, then approximately 75% of boundary length was misoriented with a common ⟨1 1 0⟩ axis after GBE. Note that by including Σ3 in this group, we are now considering misorientations outside of the fundamental zone. If other ⟨1 1 0⟩ grain boundaries are included, the total rises to 80%. The dominance of the ⟨1 1 0⟩ misorientation axis is a consequence firstly of the high fraction of Σ3 length (about 60%) and secondly of the crystallographic constraints invoked at triple junctions by multiple twinning. The majority of boundary which is misoriented on [1 1 0] is tilt in character, as shown in Fig. 4. This corroborates previous evidence from various sources that ⟨1 1 0⟩ tilt boundaries in fcc metals have lower than average energy (e.g., [16]). Here it is not only the geometrically necessary Σ27a and Σ9 misorientation that are tilt boundaries; all the misorientation angle ranges on [1 1 0] are overwhelmingly tilt in character (with the single exception of 60°/1 1 0 in GBE Ni) and furthermore encompass a range of boundary planes. This lends further support to an "energy valley" description of ⟨1 1 0⟩ tilt boundaries in general, even though, as discussed below, some particular plane combinations on either side of the boundary produce energy cusps within the valley.

It is possible to interpret and deconvolute the density distributions along the [1 1 0] zone in terms of the planes represented. The four lowest energy surface normals for fcc metals are (1 1 1), (1 0 0), (1 1 0), (1 1 3). We might therefore expect to see these planes represented. There is evidence for maxima near (1 1 1), (1 0 0) and (1 1 3), but not (1 1 0), which would have a twist component. This is consistent with the higher energy exhibited by twist boundaries compared to tilts [16]. For both Σ9 and Σ27a systems there are two symmetrical tilt grain boundaries (STGBs) – {1 1 4} and {2 2 1} for Σ9; {5 1 1} and {5 5 2} for Σ27a – and a large number of ATGBs on low- to medium-index planes. Table 1 lists these plane combinations and, for the case of Σ9, the calculated grain boundary energy for copper [17]. In theory there exists an infinite number of ATGB combinations, depending on the upper limit placed upon the Miller indices. The list in Table 1 comprises only low indices on one side of the boundary and are all of the form *hkk*/*hhk*. In several cases a high-index boundary plane is vicinal to a low-index plane, e.g., {1 1 1}/{11, 11, 1} is vicinal (3.7° deviation) to the incommensurate boundary {1 1 1}/{1 1 0}. A further important point to note is that the energy of some ATGBs in the Σ9 family, e.g., {1 1 1}/{5 1 1}, is lower than the STGBs.

As noted in the previous section, peaks for (1 1 1) and (1 1 5) planes are clearly observed on the [1 1 0] tilt zone after GBE. We can deduce from the angle between the peaks on the [1 1 0] zone that these two peaks form a population of ATGBs: (−1 −1 −5) and (1 1 1) planes constitute the ATGB for the Σ9 misorientation of 141.06°/[1 1 0]. This misorientation is symmetrically equivalent to the 38.94°/[1 1 0] disorientation. Furthermore, the energy values in Table 1 indicate that {1 1 1}/{1 1 5} is a low-energy plane combination for Σ9. A peak for the (114) STGB is also definitely present. The (1 1 4) boundary only occurs very near to the reference misorientation for nickel. For copper there is a much bigger spread of plane types than for nickel, and several other planes, e.g. {1 0 0}/{7 4 4} (or its vicinal counterpart {1 0 0}/{2 1 1}), might be included in the overlapping peaks. The Σ9 (221) STGB is not observed, presumably because it has higher energy than some other plane combinations.

Table 1
Combinations of boundary planes for STGBs and ATGBs in Σ9 and Σ27

Σ9 planes	Energy in copper [17] (mJ m^{-2})	Σ27a planes
1 1 1/5 1 1	704	5 1 1/5 1 1
1 1 4/1 1 4	704	8, 7, 7/4, 1, 1
1 0 0/7 4 4	708	5 5 2/5 5 2
2 2 1/2 2 1	756	7, 7, 1/19, 19, 13
7 5 5/7 7 1	777	2 2 1/7 4 4
1 1 1/11, 11, 1	784	7, 5, 5/29, 5, 5
2 1 1/5 5 2	786	1 1 1/11, 11, 1
2 1 1/22, 1, 1	868	13, 13, 11/19, 7, 7
1 1 0/8 7 7	905	13, 8, 8/17, 2, 2

Fig. 11 shows the frequency distribution of misorientation deviation from Σ9 in GBE Cu. It can be seen that the maximum frequency is displaced 1°–1.5° from the exact Σ value. The spread of misorientation deviation angles for Σ9 means that the deviation arises cumulatively from the two boundaries that have conjoined to form the Σ9, because in total 96% of Σ9s occur in conjunction with other $\Sigma 3^n$ boundaries at triple junctions. Fig. 8 showed statistics of triple junction constitution in the GBE specimens. In the nickel specimens 31% of junctions are Σ3–Σ3–Σ9 and 11% are Σ3–Σ9–Σ27, with similar statistics in GBE copper. Previous work has shown that often in a Σ3–Σ3–Σ9 junction one Σ3 is vicinal to the exact Σ3 misorientation [18], which feeds through to give a deviation in the conjoining Σ9 misorientation, and is in agreement with the Σ9 misorientation distribution recorded here in Fig. 11.

To summarize the data on the Σ9 subset, whereas the Σ9 population includes some boundaries with low-index planes (such as the {1 1 1}/{1 1 5} ATGB, {1 1 4} STGB) which are low-energy interfaces, other Σ9s are displaced from energy minima. This is a provocative implication because the crystallographic characteristics of the Σ9 population are thought to be a key factor in both the formation of the GBE microstructure and its subsequent properties [19].

The plane distributions for Σ27a show overlapping peaks along much of the [1 1 0] zone. The peaks in the FPGBD include the (1 1 5) STGB position, and so this boundary is likely to be present. There is no evidence for the occurrence of the other STGB in the Σ27a system, (5 5 2). Furthermore, the peaks are offset from (1 1 1) by more than 10°. Inspection of Table 1 shows that the only boundary containing a {1 1 1} plane is {1 1 1}/{11, 11, 1} and {11, 11, 1} is not present in the data. However, another ATGB in the Σ27a system is {7 7 8}/{1 1 4}, and {7 7 8} is 3.7° from {1 1 1}. A previous transmission electron microscopy study on Σ27a planes in copper showed that {7 7 8}/{1 1 4} facets occurred more frequently than any other [20]. It can be seen in Fig. 7 that the (7 7 8)/(1 1 4) ATGB is present within the broad peaks of the distribution, even though the maximum is reached near (2 2 3)/(1 1 7). As shown in Fig. 7, the Σ27b boundary population is near [1 1 0] tilt, which places it on the slope of the [1 1 0] tilt energy valley. Once again, the importance of ⟨1 1 0⟩ tilt boundaries is demonstrated.

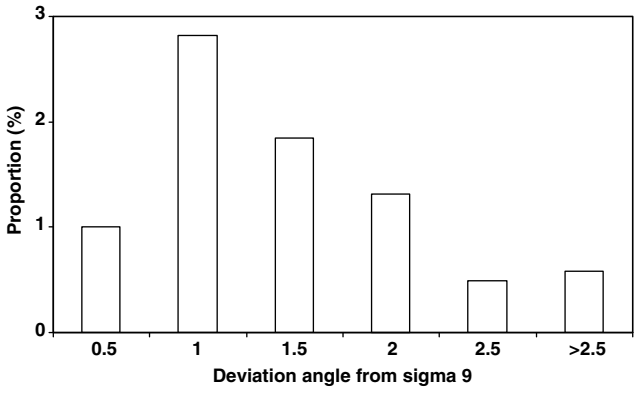

Fig. 11. Deviation from the exact misorientation angle for the Σ9 boundary population in GBE copper, up to a maximum value of 5°.

In summary, after GBE the interface population includes Σ3s, many of which are on planes vicinal to {1 1 1} and have replaced parts of the grain boundary network, plus other boundaries which are misoriented on ⟨1 1 0⟩, as governed mainly by multiple twinning. There is a clear propensity for selection of particular planes which are associated with low energy, namely ATGBs. Many of these ATGBs comprise at least one low-index plane (e.g., {1 1 1}/{1 1 5}) or are vicinal to at least one low-index plane (e.g., {7 7 8}/{1 1 4} is vicinal to {1 1 1}/{1 1 4}). Because of the constraint imposed by the misorientation geometry, both interfacing planes cannot usually have low indices. The mechanism of this type of GBE is therefore replacement of the majority of the random boundary network with corrosion resistant boundaries. The results obtained here are consistent with previous work which suggests that special behaviour at grain boundaries is related to low-index planes rather than particular misorientations [9,10]. Since many grain boundaries are curved (or faceted, particularly Σ3s), such low-index planes may reside only on parts of an interface having a particular misorientation, rather than along the whole interface. As yet, the five-parameter analysis does not provide information on the location in the microstructure of particular planes, such as those arrowed in Fig. 9d. However, even parts of an interface having low-index planes would restrict intergranular transport along the boundary.

Recently, a five-parameter analysis of brass which had been subjected to iterative thermomechanical processing was reported [12]. The processing of the brass resulted in enhanced ductility, and so the specimen had undergone a type of GBE. In the case of the processed brass the fraction of Σ3s increased greatly but on the whole these Σ3s did not become incorporated in the grain boundary network,. The five-parameter analysis of the brass specimen revealed that most of the Σ3 interface was on {1 1 1} planes, and also that there was an overall increase in ⟨1 1 0⟩ asymmetric tilt boundaries. These were explained by the restrictions at triple junctions caused by the high fraction of {1 1 1} planes. The five-parameter analyses have shown that the mechanism of GBE in the brass specimen was based on the generation of new twins. Essentially, this is mechanistically different to that observed in the present case, which relies on Σ3 regeneration and therefore replacement of the grain boundary network with Σ3s having a range of planes.

Finally, we observe that, whereas the FPGBDs for GBE nickel and copper are broadly similar, they are not identical. The stacking fault energy of copper is much lower than that of nickel (78 and 128 mJ m^{-2}, respectively) so intrinsically copper has a greater ability to form annealing twins than nickel. However, there is actually more Σ3 length in nickel than in copper after GBE, which shows that most

of the Σ3s have not resulted from new twinning. The grain size of the GBE nickel is much larger than that of copper, which may also have a bearing on the amount of Σ3 length. There are also more triple junctions with three $\Sigma 3^n$ boundaries in nickel (43%) compared to copper (38%), which is a direct result of the higher proportion of Σ3s in nickel. As discussed in detail above, there are some differences in the distribution of planes in the two metals, which underlines the fact that boundary energy is not simply related to boundary geometry alone.

5. Conclusions

An analysis of the FPGBD in GBE nickel and copper has been carried out. The main conclusions of the work are:

1. The fractional area of {1 1 1} planes after GBE was roughly constant when the entire population was considered, but decreased in the population of non-Σ3 boundaries. This decrease shows that most of the newly generated Σ3 population was not coherent annealing twins, because these would have been on {1 1 1}. Rather, they have been formed by regeneration events.
2. There was a larger proportion of Σ3 boundary length that was either vicinal-to-{1 1 1} or ⟨1 1 0⟩ type ATGB after GBE than before GBE.
3. Approximately 80% of the boundary length was misoriented on or near ⟨1 1 0⟩ after GBE. This length includes, but is not restricted to, Σ3, Σ9 and Σ27a boundaries. The majority of this boundary length was asymmetrical tilt in character, whether or not it was associated with a CSL. GBE greatly increased the proportion of $\Sigma 3^n$ triple junctions.
4. There was a clear propensity for selection of particular planes or plane combinations which are associated with low energy, namely ATGBs. Many of these ATGBs comprised at least one low-index plane or are vicinal to at least one low-index plane.
5. The GBE specimens showed an increased resistance to intergranular corrosion compared to non-GBE specimens.
6. The mechanism of GBE is replacement of the majority of the random boundary network with low-energy boundaries.

Acknowledgements

The work at Carnegie Mellon University was supported primarily by the MRSEC program of the National Science Foundation under Award Number DMR-0520425. The work at Swansea was partially supported by the Engineering and Physical Sciences Research Council.

References

[1] Randle V. Acta Mater 2004;52:4067.
[2] Viewpoint set no. 40, Scripta Mater Grain Boundary Engineering. In: Kumar M, Schuh CA, editors. vol. 54; 2006. p. 961.
[3] Palumbo P. International Patent Classification C21D 8/00 8/10 C22F 1/10 1/08, no. WO 94/14986; 1994.
[4] Randle V. Acta Mater 1999;47:4187.
[5] Reed R, Kumar M. Scripta Mater 2006;54:1029.
[6] Schuh CA, Frary M. Scripta Mater 2006;54:1023.
[7] Randle V, Davies P Hulm B. Philos Mag 1999;79A:305.
[8] Wolf U, Ernst F, Muschik T, Finnis MW, Fischmeister HF. Philos Mag 1992;66A:991.
[9] Saylor DM, Adams BL, El-Dasher BS, Rohrer GS. Metall Mater Trans 2003;34A:1.
[10] Saylor DM, Morawiec A, Rohrer GS. Acta Mater 2003;51:3663.
[11] Saylor DM, El-Dasher BS, Rollett AD, Rohrer GS. Acta Mater 2004;52:3649.
[12] Randle V, Rohrer GS, Kim C, Hu Y. Acta Mater 2006;54:4489.
[13] <http://www.integran.com/tech/gbe.htm>.
[14] Was GS, Alexandreanu B. Scripta Mater 2006;54:1047.
[15] Tan L, Sridharan K, Allen TR. J Nucl Mater 2007;371:171–5.
[16] Wolf D. Acta Metall Mater 1990;38:791.
[17] Merkle KL, Wolf D. Philos Mag 1992;65A:513.
[18] Randle V, Hu Y. J Mater Sci 2005;40:3243.
[19] Gertsman VY. Acta Cryst 2001;A57:649.
[20] Sukholmin GD, Andreeva AV. Phys Status Solidi 1983;78A:333.